Bioconjugate Chemistry

pubs.acs.org/bc

Article

Multifunctional Nanozyme Hydrogel with Mucosal Healing Activity for Single-Dose Ulcerative Colitis Therapy

Chaoqun Cheng, Yuan Cheng, Sheng Zhao, Quan Wang, Sirong Li, Xiwen Chen, Xiaohan Yang, and Hui Wei*

Cite This: *Bioconjugate Chem.* 2022, 33, 248−259

Read Online

ACCESS | Metrics & More | Article Recommendations | Supporting Information

ABSTRACT: Nanozymes are nanomaterials with enzyme-like activities, which have been developed for inflammatory disease therapy by reactive oxygen species (ROS) scavenging. The application of nanozymes in ulcerative colitis (UC) treatment not only inherits the merits of small molecular antioxidants (*e.g.,* 5-aminosalicylic acid) to scavenge ROS but also achieves catalytic recycle instead of stoichiometric consumption. However, current therapies usually ignore the repair of mucosa, the first line of defense, whose damage increases the risk of infections. Herein, a multifunctional nanozyme hydrogel is designed and verified both as an ROS scavenger and a mucosal healing enhancer for UC therapy. The chitosan-coated CeO_2 nanozyme (CCNZ) not only possesses excellent ROS-scavenging ability but also exhibits satisfactory antibacterial capacity. After gelation with alginate, the optimized $CCNZ_1$:$Alg_{1.5}$ nanozyme hydrogel exhibits multiple functions, including inflamed site targeting, supporting cell growth, ROS scavenging, and antibacterial activity, which alleviates UC better than a clinical medication 5-aminosalicylic acid by even a single-dose treatment. This study reveals that a nanozyme providing mucosal healing is promising for UC therapy with excellent potential for clinical application and enriches the nanozyme research of treatment for diseases.

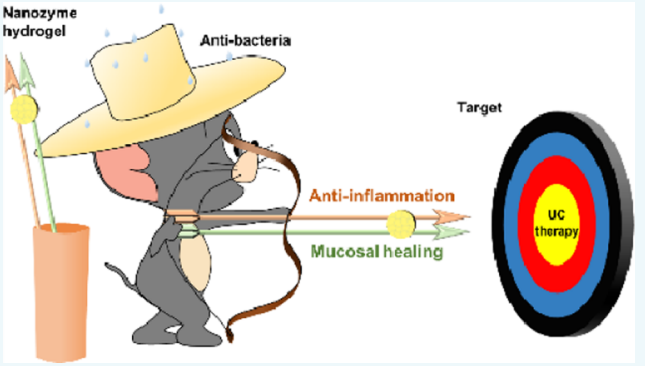

INTRODUCTION

Ulcerative colitis (UC), one of the typical inflammatory bowel diseases, is a chronic inflammatory disease accompanied by weight loss, rectal bleeding, diarrhea, and abdominal pain.[1] After the mucosal barrier is disrupted in the gut, the innate immune cells, such as polymorphonuclear leukocytes, macrophage, and lymphocyte, migrate to inflamed sites, which engulf invading pathogens and release reactive oxygen species (ROS).[2] However, persistent oxidative stress with uncontrolled overproduction of ROS will result in tissue injury, leading to the initiation and progression of UC.[3] Until now, almost 60% of UC patients have received oral treatment with 5-aminosalicylic acid (5-ASA), which has shown antioxidation activities to various degrees.[4,5] Although it is a conventional drug for UC therapy, the side effects from 5-ASA generally hinder the sufficient doses to ensure the efficacy.[6] Moreover, the lack of inflamed site targeting results in the further decrease of therapeutic concentration in the gut. Therefore, new therapeutics are urgently needed for UC therapy.

Recently, nanozymes have attracted much attention in various disease therapies including UC therapy, which can catalytically scavenge ROS with their intrinsic enzyme-like activities.[7] For example, Prussian blue and Mn_3O_4 nanozymes with multiple enzyme-like activities have been fabricated to effectively relieve colitis.[8] The Pt@PCN222-Mn nanozyme was designed to mimic the superoxide dismutase (SOD)/catalase (CAT) cascade reactions for better ROS elimination and achieved effective colitis therapy.[9] Meanwhile, to improve gut specificity, negatively charged nanozymes were designed to target the inflamed colonic epithelium which is characterized with the accumulation of positively charged proteins.[10−12] For instance, the negatively charged ceria nanozyme grown on sheets of montmorillonite was able to target the inflamed colonic sites for UC therapy.[12] While these studies have shown the promising therapeutic efficacy of nanozymes because of their advantages over natural enzymes or antioxidant drugs, the mucosal healing has not been achieved with nanozymes yet in UC therapy.[13]

Mucosal inflammation is observed in about 45% of patients with UC in clinical remission,[14] which could be attributed to the ROS-induced inflammation and the activity loss of

Received: December 10, 2021
Revised: December 11, 2021
Published: December 22, 2021

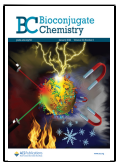

Scheme 1. Schematic Illustration of the Multifunctional Nanozyme Hydrogel for UC Therapy[a]

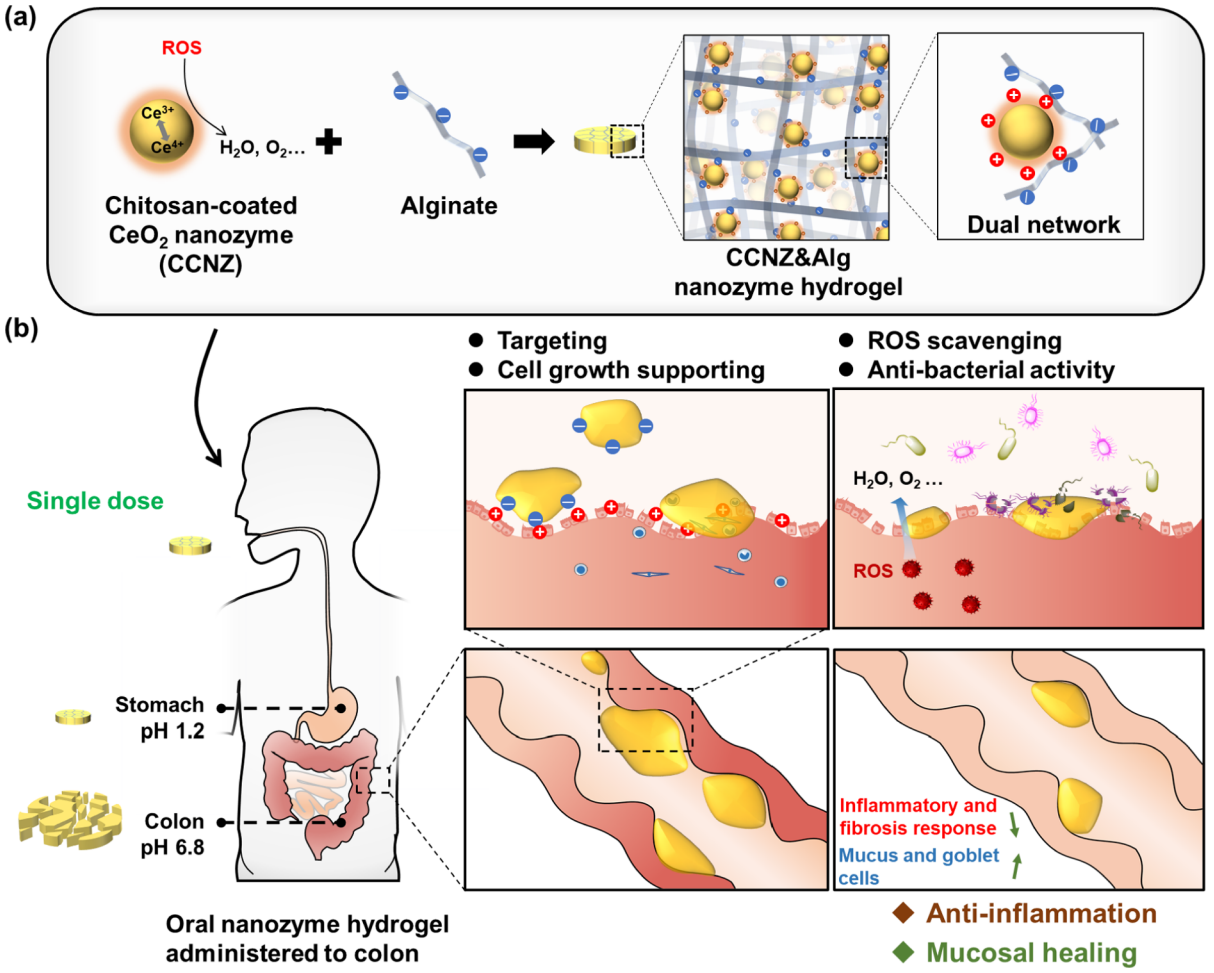

[a](a) Fabrication of the CCNZ&Alg Nanozyme Hydrogel and (b) Oral Administration of the CCNZ&Alg Nanozyme Hydrogel for Effective UC Therapy Based on Its Multiple Functionalities

epithelial antimicrobial peptides.[15] Mucosal healing is considered as a crucial endpoint in the treatment of UC patients.[13,16] Therefore, it is necessary to design nanozymes with mucosal healing activity for better UC therapy. To fulfill this need, herein we reported the development of a CeO_2-encapsulated chitosan (Cs) and alginate (Alg) hydrogel (CCNZ&Alg). To distribute CeO_2 uniformly, we designed a Cs-coated CeO_2 nanozyme (CCNZ), which maintained the SOD- and CAT-like activities of the pristine nanozyme and would eliminate excessive ROS and exert antibacterial activity.[17] After gelation with Alg, the dual-crosslinked hydrogel CCNZ&Alg would not only provide an extracellular matrix-like microenvironment to favorably support cell growth for mucosal healing but also enable the inflamed site targeting because of its overall negative charges (Scheme 1). Additionally, the nanozyme hydrogel was stable in stomach and would gradually degrade in colon after oral administration. Encouragingly, a single-dose treatment with the nanozyme hydrogel achieved better therapeutic efficacy than 5-ASA under the same dosage, demonstrating the promise of combining anti-inflammation with promoted mucosal healing in UC therapy.

RESULTS AND DISCUSSION

Synthesis and Characterizations of the Chitosan-Coated CeO_2 Nanozyme. The CeO_2 nanozyme was chosen in this work because of its several advantages compared with other nanozymes, such as multienzyme-mimicking activities; good stability in stomach after oral administration; and satisfactory biocompatibility. The CeO_2 nanozyme was prepared using the NH_4OH precipitation method and further coated with Cs (Figure 1a). The chitosan-coated CeO_2 nanozyme was designated as CCNZ. The formation of CCNZ was confirmed by transmission electron microscopy (TEM) imaging, showing uniform and discrete CCNZ with a particle size of about 5 nm (Figure 1b). A hydrodynamic diameter of about 10 nm in aqueous solution was observed (Figure S1). The crystalline features of CCNZ were characterized by using X-ray diffraction (XRD). As shown in Figure 1c, the characteristic peaks of CeO_2 (2θ = 28.5, 32.9, 47.4, and 56.8°)[18] were observed, further confirming the successful synthesis. Figure 1d shows the thermogravimetric analysis (TGA) curve of CCNZ in the range of 100−850 °C under a nitrogen atmosphere. The result was consistent with the inductively coupled plasma (ICP) characterization that the content of CeO_2 in CCNZ was 60 wt % (Table S1). In addition, the Fourier-transform infrared (FT-IR) spectra (Figure 1e) showed characteristic peaks of Cs at 3445 (ν_{OH} and ν_{NH} absorptions), 1076 (C−N stretching vibration), and 1029 cm^{-1} (C−O−C stretching vibration) from CCNZ, demonstrating the successful coating of Cs and the intact

https://doi.org/10.1021/acs.bioconjchem.1c00583
Bioconjugate Chem. 2022, 33, 248−259

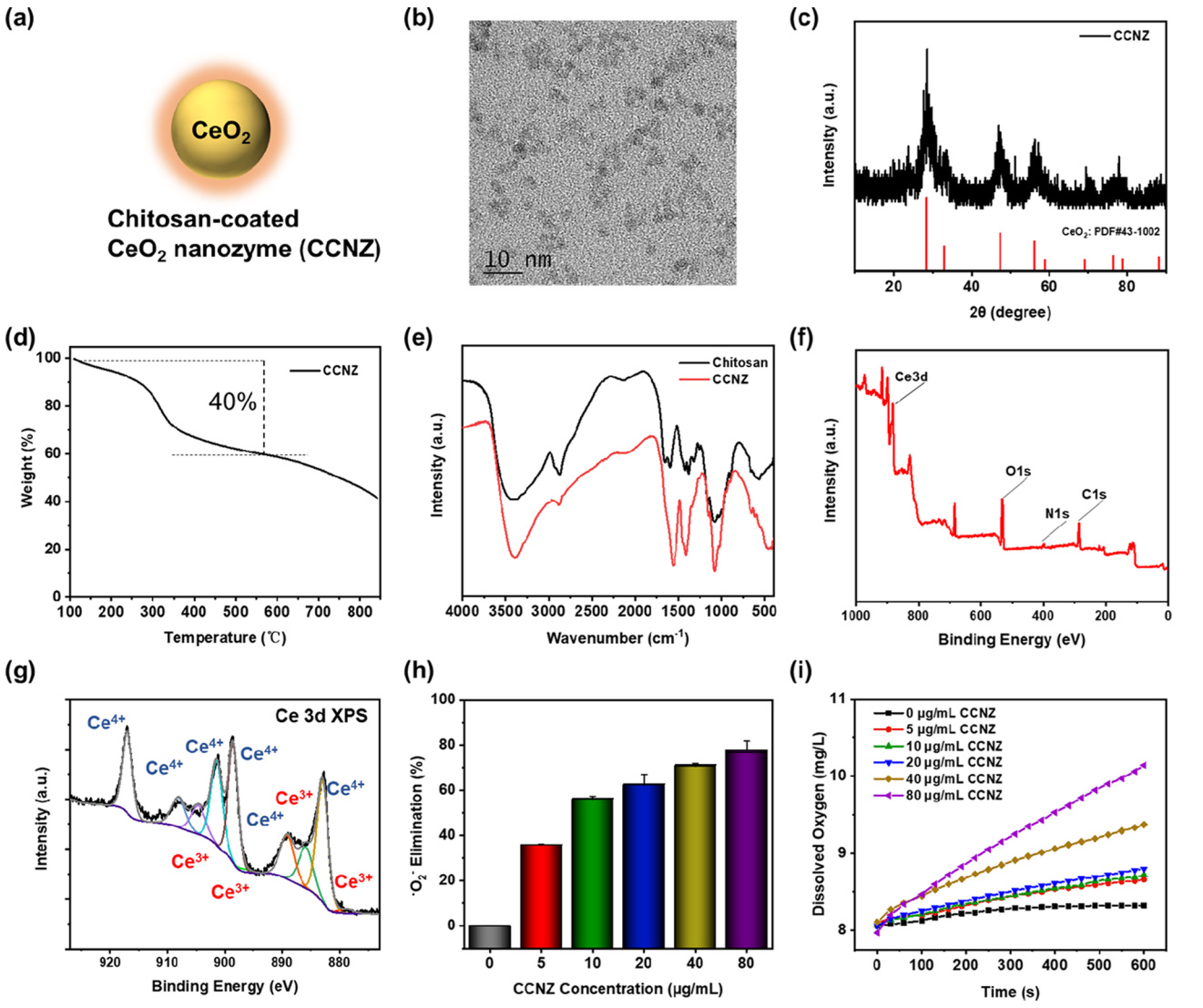

Figure 1. Characterizations of CCNZ and catalytic activities. (a) Schematic of CCNZ. (b) TEM image of CCNZ. (c) XRD pattern of CCNZ. (d) TGA curve of CCNZ. (e) FT-IR spectra of indicated materials. (f) X-ray photoelectron spectroscopy (XPS) survey spectrum and (g) Ce 3d XPS spectrum of CCNZ. (h) Dependence between the elimination efficiency of $^{\bullet}O_2^-$ and concentrations of CCNZ by SOD-like activity. (i) Dissolved oxygen from different concentrations of CCNZ with 5 mM H_2O_2 by CAT-like activity, respectively.

structure of Cs after coating. The ratio of Ce^{3+} and Ce^{4+} on the surface of CCNZ was calculated according to X-ray photoelectron spectra because the enzyme-like activities are dependent on it. As shown in Figure 1f,g, CCNZ showed a high ratio of Ce^{3+} on the surface. It confirms the presence of both valences on CCNZ, which was not obviously influenced by the coating with Cs. In addition, the elements on the surface of CCNZ contain C, N, O, and Ce.

ROS-Scavenging Activities of CCNZ. CeO_2 nanoparticles can be coated by polymers with different terminal groups, which influence the functions of nanoparticles and tune the enzyme-like activities for biomedical applications.[19] Therefore, the ROS-scavenging activity of CCNZ was further investigated. First, the SOD-like activity was correlated with the elimination of $^{\bullet}O_2^-$, which was generated from riboflavin with light irradiation. As shown in Figure 1h, the $^{\bullet}O_2^-$-scavenging activity of CCNZ exhibited a dose-dependent manner, and the $^{\bullet}O_2^-$ elimination of 80 μg/mL CCNZ was close to 80% compared with that of the control group. In addition, Figure S2a shows that the $^{\bullet}O_2^-$ elimination capacity of CCNZ was close to citric acid-coated CeO_2 which has been reported.[20] The CAT-like activity of CCNZ was investigated by monitoring the dissolved O_2 from H_2O_2 decomposition, which exhibited time−concentration dependency relation (Figure 1i), increased by the reaction with H_2O_2. The H_2O_2 elimination of 80 μg/mL CCNZ was close to 60% compared with that of the control group (Figure S2b,c). These results showed that CCNZ retained the excellent SOD- and CAT-like activities of pristine CeO_2.

Negative Surface Charge and Antibacterial Ability of the Nanozyme Hydrogel. To increase the efficiency of inflammation targeting, the surface charge of the nanozyme hydrogel should be regulated to the negative charges, which facilitated adhesion to the inflamed colonic sites with positive charges. The positive charges can be attributed by the cationic proteins attached on the inflamed colonic sites after the damage of the mucosal barrier.[10] Meanwhile, the infectious risks should also be inhibited during UC therapy.[21] We hypothesized that the negatively charged surface and antibacterial effects of the nanozyme hydrogel not only exhibit

https://doi.org/10.1021/acs.bioconjchem.1c00583
Bioconjugate Chem. 2022, 33, 248−259

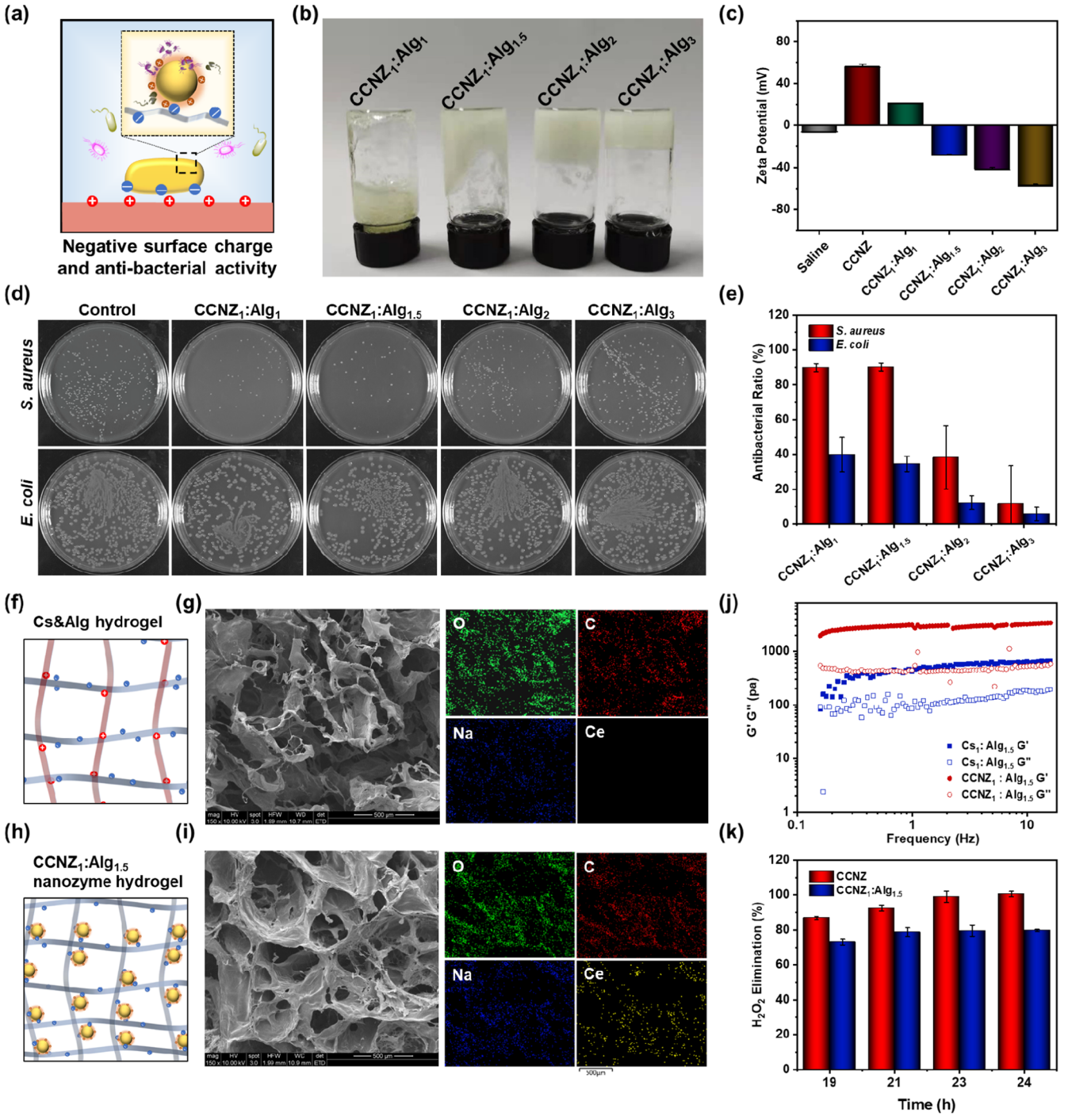

Figure 2. Optimal formulation of the nanozyme hydrogel. (a) Schematic diagram of the optimal formulation of the nanozyme hydrogel (negative surface charge and antibacterial activity). (b) Photograph of indicated hydrogels. (c) Zeta potential of indicated hydrogels. (d) Digital photographs of the remaining bacteria-inoculated agar plates and (e) corresponding antibacterial ratio after the treatment of different nanozyme hydrogels ($CCNZ_1$:Alg_1, $CCNZ_1$:$Alg_{1.5}$, $CCNZ_1$:Alg_2, and $CCNZ_1$:Alg_3). (f,h) Schematic diagram of the nanozyme hydrogel forming tight arrangement by double crosslinking. (g,i) SEM and EDS images of the Cs&Alg hydrogel and $CCNZ_1$:$Alg_{1.5}$ nanozyme hydrogel. (j) Dynamic frequent sweeps of the nanozyme hydrogel. (k) H_2O_2 elimination of $CCNZ_1$:$Alg_{1.5}$ at 19−24 h. Data are presented as mean ± standard error of the mean (n = 4).

mucosal targeting capacity for increasing intestinal adsorption but also decrease the infectious risks (Figure 2a). After regulating the ratio of CCNZ and alginate, the nanozyme hydrogel with different formulations ($CCNZ_1$:Alg_1, $CCNZ_1$:$Alg_{1.5}$, $CCNZ_1$:Alg_2, and $CCNZ_1$:Alg_3) were formed (Figure 2b). We measured the zeta potential and antibacterial ability of these hydrogels. As shown in Figure 2c, the zeta potentials of CCNZ and $CCNZ_1$:Alg_1 were positive (+56.23 ± 2.06 and +21.2 ± 0.1 mV, respectively), while the zeta potentials of $CCNZ_1$:$Alg_{1.5}$, $CCNZ_1$:Alg_2, and $CCNZ_1$:Alg_3 were all negative charges (−28.1 ± 1.01, −41.9 ± 1.57, and −57.3 ± 1.19 mV, respectively). Overall, with decreasing the ratio of CCNZ, the negative charge increased. It was observed that $CCNZ_1$:Alg_1 and $CCNZ_1$:$Alg_{1.5}$ nanozyme hydrogels have superior antibacterial effects for *Staphylococcus aureus* and slightly antibacterial effects for *Escherichia coli* compared with

https://doi.org/10.1021/acs.bioconjchem.1c00583
Bioconjugate Chem. 2022, 33, 248−259

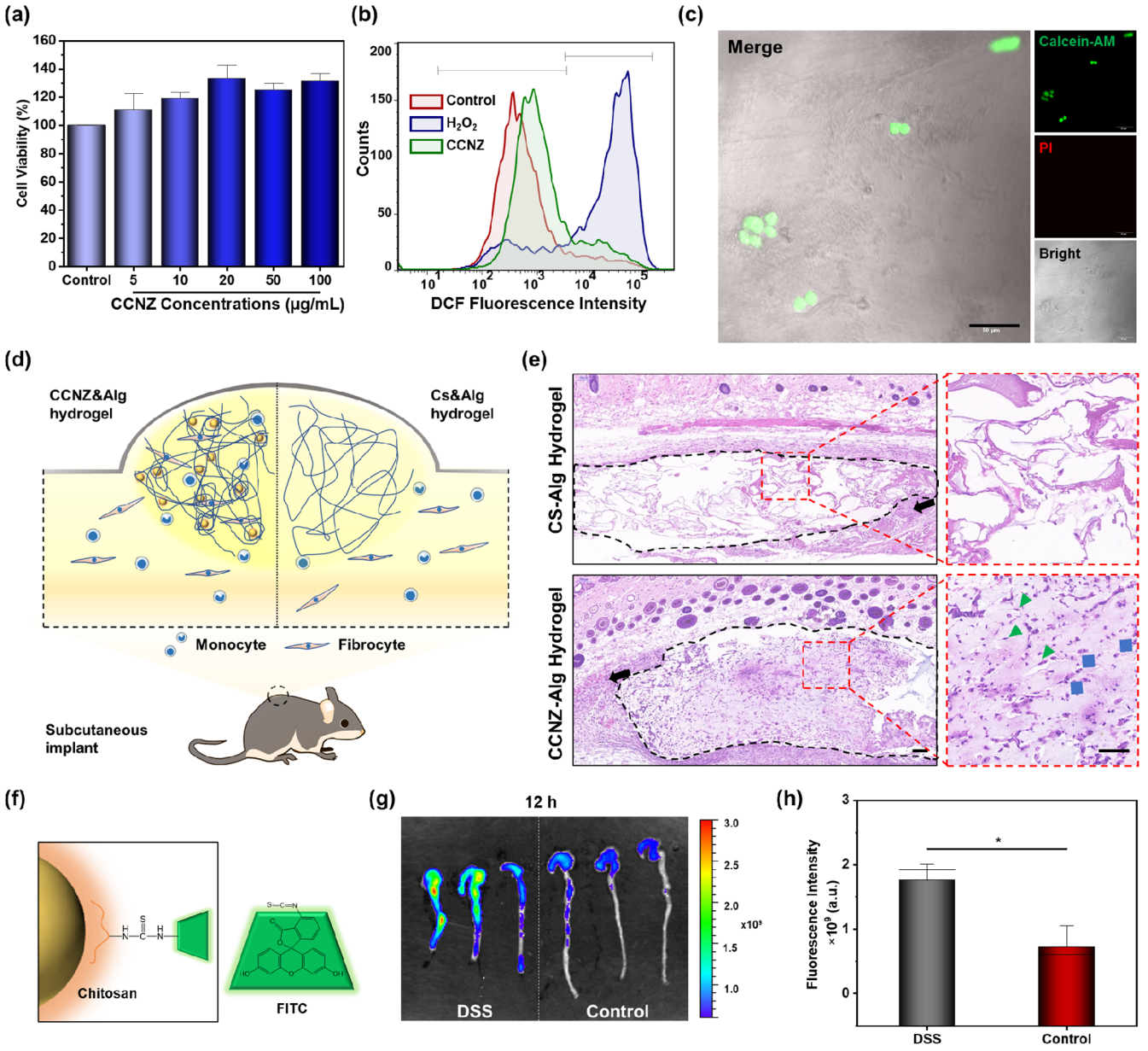

Figure 3. Biocompatibility and multifunctionality of the $CCNZ_1$:$Alg_{1.5}$ nanozyme hydrogel. (a) Cell viability of RAW 264.7 cells after being incubated with different concentrations of CCNZ. (b) Flow cytometry profiles of RAW 264.7 cells, treated with complete medium (control), H_2O_2, or CCNZ followed by H_2O_2. DCFH-DA is an ROS sensitize fluorescence probe. DCFH-DA is oxidized into fluorescent probe DCF by ROS. (c) Confocal images of RAW 264.7 cells seeded on the $CCNZ_1$:$Alg_{1.5}$ nanozyme hydrogel, stained by Calcein-AM/PI, to evaluate the cytocompatibility of the hydrogel. Scale bar: 50 μm. (d) Schematic diagram of the subcutaneous implant comparing two different hydrogels. (e) H&E-stained images of skin tissues after subcutaneously implanting the Cs&Alg hydrogel and $CCNZ_1$:$Alg_{1.5}$ nanozyme hydrogel. Hydrogel: black dashed box; inflammatory responses: pointed with black arrows; immune cells: pointed with blue square; and fibrocyte cells: pointed with green triangle. Scale bar: 50 μm. (f) Illustration of CCNZ-grafted FITC. (g) Fluorescence images of colon after treatment with the FITC-conjugated $CCNZ_1$:$Alg_{1.5}$ nanozyme hydrogel for 12 h and (h) corresponding fluorescence intensity. Data are presented as mean ± standard error of the mean (n = 3). *P < 0.05 *vs* the DSS group.

the control group (Figure 2d,e). Note that the antibacterial effect of CCNZ was concentration-dependent (Figure S3), demonstrating that chitosan still exhibits an excellent antibacterial effect after coating. Therefore, combining the results of zeta potential and antibacterial properties, $CCNZ_1$:$Alg_{1.5}$ was chosen as the optimal nanozyme hydrogel for further investigation.

The detailed structure of $CCNZ_1$:$Alg_{1.5}$ was then studied. The Cs&Alg hydrogel was also studied as a comparison. The scanning electron microscopy (SEM) images of the cross sections of the Cs&Alg hydrogel and $CCNZ_1$:$Alg_{1.5}$ nanozyme hydrogel are shown in Figure 2f–i. The internal morphologies of the hydrogels were observed. Interestingly, the $CCNZ_1$:$Alg_{1.5}$ nanozyme hydrogel was more compact than Cs&Alg, which was due to the multivalent chelation between metal nanoparticle chelate alginate.[22] The nanozyme hydrogel formed a tight arrangement by double crosslinking, resulting in smaller voids compared with the Cs&Alg hydrogel. In addition, the corresponding energy-dispersive spectroscopy (EDS) elemental mapping confirmed that the elements of O, C, Na,

https://doi.org/10.1021/acs.bioconjchem.1c00583
Bioconjugate Chem. 2022, 33, 248−259

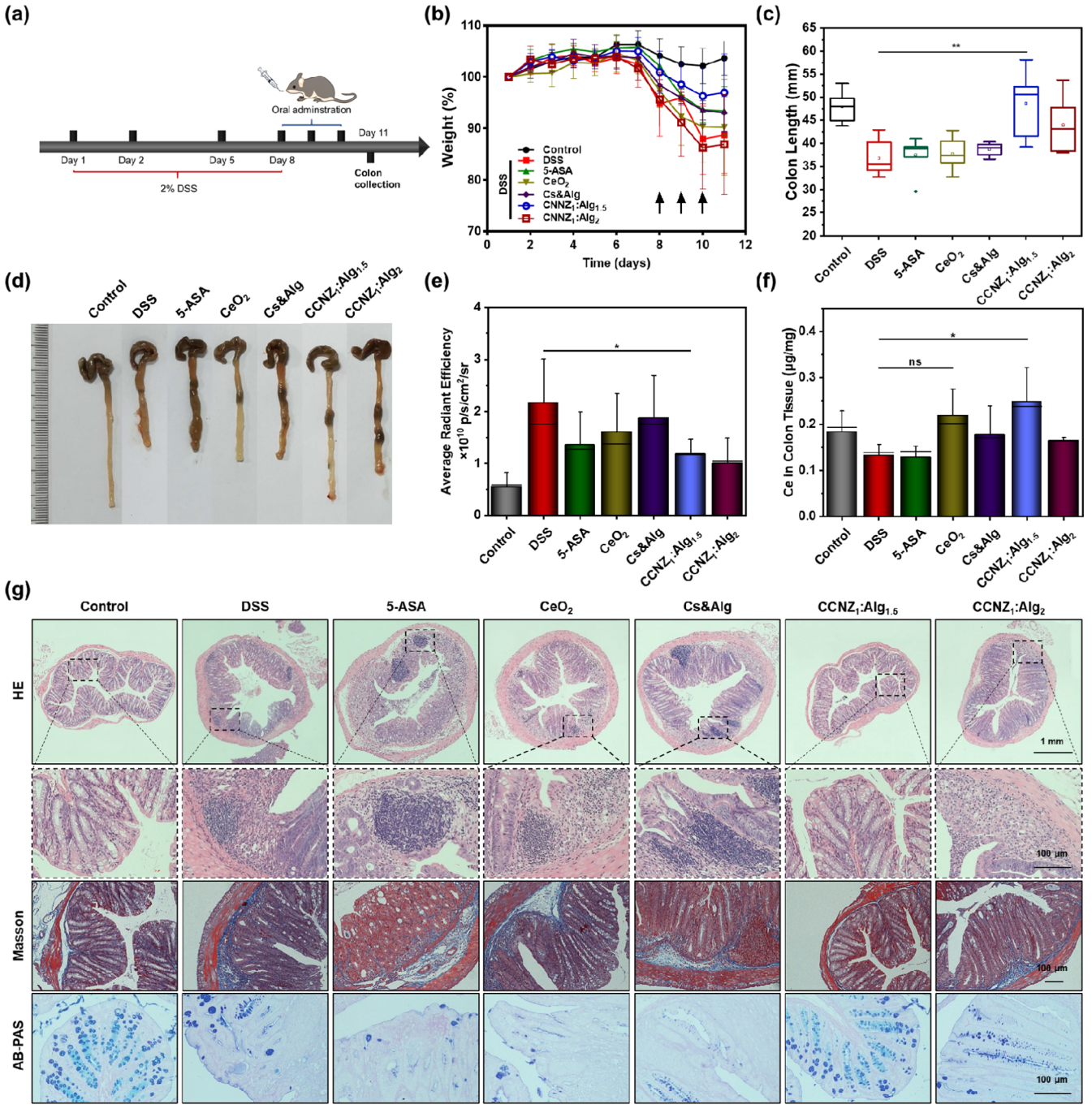

Figure 4. UC therapy with the nanozyme hydrogel compared with 5-ASA. (a) Illustration of DSS-induced UC mouse model and administration. (b) Daily body weight recorded over 11 days under different treatments. (c) Colon length of indicated treatments. (d) Representative images of colons of all treatment groups. (e) Fluorescence intensity of colon 0.5 h after injecting 0.7 mg of DCFH-DA per mouse. (f) Ce element contents from the colon of indicated treatments. (g) Histological examination of indicated treatments, H&E-, Masson's trichrome-, and AB-PAS-stained pathological colonic sections of mice. Scale bar: 1 mm; and 100 μm. Data are presented as mean ± standard error of the mean ($n = 6$). *$P < 0.05$ *vs* DSS group, ** means $P < 0.01$ *vs* DSS group. Ns means no significance.

and Ce are dispersed uniformly in the nanozyme hydrogel. Figure S4 shows that the weight percentage ratio of Ce is 14.3 wt % in the $CCNZ_1$:$Alg_{1.5}$ nanozyme hydrogel, which is close to the theoretical value (19.4%, Table S1). Meanwhile, the storage modulus (G') and loss modulus (G'') were monitored over the frequency sweep (Figure 2j). It suggests that the G' values are larger than G'' values for both Cs&Alg and CCNZ&Alg, confirming the formation of elastic hydrogels. Also, the G'/G'' values of the $CCNZ_1$:$Alg_{1.5}$ nanozyme hydrogel are larger than those of the Cs&Alg hydrogel, indicating that $CCNZ_1$:$Alg_{1.5}$ has better mechanical properties. The result was consistent with SEM imaging, which showed that the double network is formed in the nanozyme hydrogel. To investigate whether the formation of the hydrogel affects the catalytic activity of CCNZ, the H_2O_2 elimination of $CCNZ_1$:$Alg_{1.5}$ was examined. As shown in Figure 2k, identical efficiency of $CCNZ_1$:$Alg_{1.5}$ compared with that of CCNZ was observed at 19−24 h, and a slightly lower efficiency of the

https://doi.org/10.1021/acs.bioconjchem.1c00583
Bioconjugate Chem. 2022, 33, 248−259

former was observed at 1−6 h (Figure S5), which demonstrated the retained ROS-scavenging activities. In practice, the nanozyme hydrogel has to stay in stomach for several hours. Therefore, the nanozyme hydrogel was kept in 0.9% NaCl (pH 1.2) for 4 h, and then, the H_2O_2 elimination efficiency was measured under neutral conditions (Figure S6). The result shows that the enzyme-like activity would not be influenced after passing through stomach, showing the possibility for oral administration.

Biocompatible and Multifunctional $CCNZ_1$:$Alg_{1.5}$ Nanozyme Hydrogel. The cell viability of CCNZ and nanozyme hydrogels toward RAW 264.7 was determined to investigate their biocompatibility by using CCK8 (Cell Counting Kit-8) assays. Figure 3a shows that CCNZ did not inhibit the growth of RAW 264.7 cells within 100 μg/mL after coculture for 1 day. In addition, the transwell cell culture system was used to evaluate the potential cytotoxicity of the nanozyme hydrogel, as shown in Figure S7a. The result of Figure S7b indicates that no cytotoxicity was observed for nanozyme hydrogels of 1 or 10 mg/mL. Based on the excellent biocompatibility, we further examined the ROS-scavenging ability in cultured RAW 264.7 cells. Cells were incubated with CCNZ for 2 h, followed by 30 min of incubation with H_2O_2. The intracellular ROS level was then monitored by using a ROS-sensitive probe [2′,7′-dichlorofluorescin diacetate (DCFH-DA)] and evaluated by using laser scanning confocal microscopy (Figure S8) and flow cytometry (Figure 3b), respectively. In the presence of ROS, the nonfluorescent probe (DCFH) was oxidized into its fluorescent form [2′,7′-dichlorofluorescein (DCF)].[23] After being treated with H_2O_2, the green DCF fluorescence represents the content of ROS in cells. The ROS level after CCNZ treatment was less than that of the H_2O_2 group, indicating that CCNZ can reduce the cellular ROS level and protect them from ROS injury, which benefits cell proliferation and growth in UC therapy. Generally, the sustained release of CCNZ from the nanozyme hydrogel in a physiological environment is shown in Figure S9. After being covalently grafted with the fluorescein isothiocyanate (FITC) fluorescence probe, the released CCNZ was monitored by using laser scanning confocal microscopy and flow cytometry, respectively. The fluorescence intensity of CCNZ in cells increased over time after being treated for 0−100 min. In addition, based on fluorescence image analysis, the released CCNZ was uptaken by RAW 264.7 cells.

To further investigate the growth of cells in the nanozyme hydrogel, RAW 264.7 cells were directly seeded on the $CCNZ_1$:$Alg_{1.5}$ nanozyme hydrogel. Calcein-AM/PI staining (Figure 3c) illustrated the live/dead cells after culturing on the nanozyme hydrogel for 1 day. The results show that the majority of cells were stained in green (live cells), and few cells were stained in red (dead cells), indicating that cells were growing well on the $CCNZ_1$:$Alg_{1.5}$ nanozyme hydrogel. Meanwhile, RAW 264.7 cells cocultured with the $CCNZ_1$:$Alg_{1.5}$ nanozyme hydrogel in the transwell cell culture system, and the results of Calcein-AM/PI staining show excellent cytocompatibility (Figure S7c). Furthermore, as shown in Figure 3d, subcutaneously implanted $CCNZ_1$:$Alg_{1.5}$ nanozyme hydrogel was used to demonstrate the host inflammatory response and the ability of cell growth *in vivo*. The samples were extracted after 7-day postimplantation and examined histologically. Hematoxylin and eosin (H&E) staining (Figure 3e) showed mild inflammatory responses that occurred in two groups (pointed with black arrows), indicating the typical foreign body response without excessive inflammation. Moreover, the $CCNZ_1$:$Alg_{1.5}$ nanozyme hydrogel (black dashed box) maintained structural integrity and filled with cells including immune cells (pointed with blue square) and fibrocyte cells (pointed with green triangle), revealing that the robust mechanical structure provided a suitable microenvironment to the cells. In general, the $CCNZ_1$:$Alg_{1.5}$ nanozyme hydrogel not only exhibited excellent cytocompatibility but also provided a robust mechanical microenvironment to support cell growth, compared with the Cs&Alg hydrogel. In addition, the negative surface charge of the $CCNZ_1$:$Alg_{1.5}$ nanozyme hydrogel is able to target and adhere to the positively charged surface of inflamed colon epithelium. Fluorescent CCNZ was then obtained by covalently conjugating FITC to the NH_2 groups of the CCNZ (Figure 3f). Preferentially targeted and adhered to inflamed mucosa was further validated *in vivo*. Dextran sulfate sodium (DSS)-induced mice and untreated healthy control mice were orally administrated with the FITC-conjugated $CCNZ_1$:$Alg_{1.5}$ nanozyme hydrogel, sacrificed 12 (Figure 3g) and 24 h (Figure S10) later, respectively, and the fluorescence intensity was quantified (Figure 3h). The DSS group showed a higher fluorescence intensity than the control group, demonstrating more nanozyme hydrogel adhesion. It is obvious that the nanozyme hydrogel enhances the residence time in UC therapy. In short, the UC-targeting nanozyme hydrogel with satisfactory biosafety has been obtained and verified.

***In Vivo* UC Therapy.** Based on the multifunctional nanozyme hydrogel, including ROS scavenging, antibacterial activity, excellent biocompatibility, inflamed site targeting, and cell growth supporting, the acute DSS-induced UC model was utilized to investigate the therapeutic efficacy. As shown in Figure 4a, mice were subjected 8 days to drinking water containing 2% (w/v) DSS, which directly causes toxicity to colonic epithelial cells and compromises mucosal barrier,[24] followed by the oral administration of CeO_2, Cs&Alg hydrogel, 5-ASA, $CCNZ_1$:$Alg_{1.5}$, and $CCNZ_1$:Alg_2 nanozyme hydrogel, respectively, once a day for 3 consecutive days (days 8, 9, and 10). 5-ASA is a first-line medication for UC therapy, which can remarkably suppress ROS.[4] Meanwhile, the $CCNZ_1$:Alg_2 nanozyme hydrogel has a lower ratio of CCNZ than the $CCNZ_1$:$Alg_{1.5}$ nanozyme hydrogel. After that, the colon was collected, the length of which and pathological studies were analyzed to study the therapeutic efficacy. The body weight of all groups was recorded during the whole experiment, and the result shows that the weight of healthy mice increased, while that of all DSS-induced mice decreased, as shown in Figure 4b, demonstrating the successful onset of UC. After treatment for 3 days, the body weight of mice treated with the $CCNZ_1$:$Alg_{1.5}$ nanozyme hydrogel gradually recovered. Besides, all DSS-induced mice showed shortened colon length, but the $CCNZ_1$:$Alg_{1.5}$ nanozyme hydrogel exhibited significant protection against the shortening of colon length, and the $CCNZ_1$:Alg_2 nanozyme hydrogel also slightly protected from shortening. The colon lengths of other groups (i.e., 5-ASA, CeO_2, and Cs&Alg hydrogel) were similar to those of the DSS group (Figure 4c), and the representative images and all images of colon are shown in Figures 4d and S11. In addition, consistent with the *ex vivo* fluorescence intensity of colon after intraperitoneal injection of 0.7 mg DCFH-DA per mouse (Figures 4e and S12), the DSS-induced groups showed high intensity, while the $CCNZ_1$:$Alg_{1.5}$ nanozyme hydrogel

https://doi.org/10.1021/acs.bioconjchem.1c00583
Bioconjugate Chem. 2022, 33, 248−259

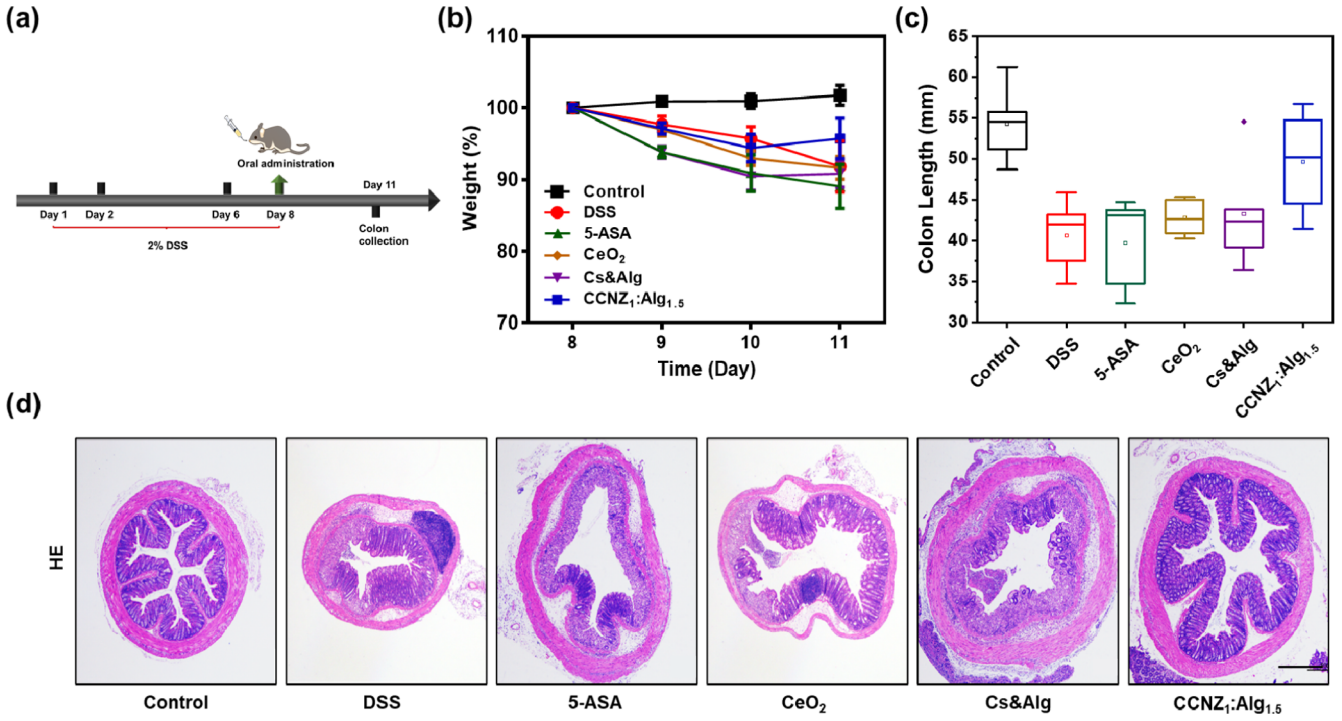

Figure 5. Single dose of treatment. (a) Illustration of the DSS-induced UC mouse model and administration of single dose. (b) Daily body weight recorded after indicated treatments. (c) Colon length of indicated groups. (d) H&E-stained pathological colonic sections of mice from indicated groups on day 11. Scale bar: 1 mm. Data are presented as mean ± standard error of the mean (n = 5).

significantly decreased average radiant efficiency. This result demonstrated that the inflammatory response was effectively alleviated after ROS scavenging by the nanozyme. Moreover, as shown in Figure 4f, more abundant Ce was examined in the colon after being treated with the $CCNZ_1$:$Alg_{1.5}$ nanozyme hydrogel compared to the CeO_2 group, indicating that the nanozyme hydrogel efficiently adhered to inflamed mucosa and exerted healing efficacy. The result is in accordance with the fluorescence images of colon after treatment with the FITC-conjugated $CCNZ_1$:$Alg_{1.5}$ nanozyme hydrogel as mentioned above (Figure 3f–h).

Besides, to further evaluate the therapeutic efficacy, the histological examination was performed and the results are shown in Figure 4g. H&E staining indicated the presence of severe glandular defects, inflammatory cell infiltration, and mucosal ulceration in the inflamed colon sections after DSS treatment. In contrast, lots of intestinal crypts present a single straight tubular gland with intact structures, which are open to the mucosal surface in the control group. Compared with the DSS group as well as the other treated groups, the $CCNZ_1$:$Alg_{1.5}$ nanozyme hydrogel group exhibited much lower inflammatory cell infiltration and had a sound structure. Besides, fibrosis response in the DSS-induced UC model was shown by Masson's trichrome staining.[25] In the DSS group, much collagen deposition (blue) was observed. However, the areas of collagen deposition were meekly decreased after nanozyme hydrogel treatment. Importantly, the goblet cells and mucus were stained by Alcian blue-periodic acid-Schiff (AB-PAS) staining to investigate their integrity. Goblet cells secrete mucus that have a well-appreciated role in barrier maintenance, preventing pathogens from invading the mucosa to cause intestinal inflammation. The numbers of goblet cells and mucous thickness were significantly decreased in DSS-induced colitis. Among all the treatment groups, the numbers of goblet cells and mucous thickness were recovered after $CCNZ_1$:$Alg_{1.5}$ nanozyme hydrogel treatment. As previously mentioned, it is important to consider mucosal healing in UC, and the $CCNZ_1$:$Alg_{1.5}$ nanozyme hydrogel shows an excellent ability to promote mucosal healing. In short, the $CCNZ_1$:$Alg_{1.5}$ nanozyme hydrogel not only targeted to inflamed colon and decreased inflammatory response but also promoted mucosal healing. Notably, there was no obvious histological abnormality of viscera (heart, liver, spleen, lung, and kidney) after therapy, suggesting that the nanozyme hydrogel possessed good histocompatibility (Figure S13).

$CCNZ_1$:$Alg_{1.5}$ Nanozyme Hydrogel for Single-Dose UC Therapy. Clinically, reduction of treatment frequency and dose is an approaching way to lower the incidence of side effects. Based on the excellent therapeutic efficacy of the $CCNZ_1$:$Alg_{1.5}$ nanozyme hydrogel, we further studied whether a single-dose treatment could also relieve the UC. Mice were subjected 8 days to drinking water containing 2% (w/v) DSS as the same method as mentioned above (Figure 5a). After single-dose administration, the body weight of all groups was recorded (Figure 5b). The result showed that treatment with the $CCNZ_1$:$Alg_{1.5}$ nanozyme hydrogel gradually relieved the UC. Excitingly, the $CCNZ_1$:$Alg_{1.5}$ nanozyme hydrogel still protects against shortening of the colon length (Figure 5c), as demonstrated by the corresponding images of colon in Figure S14. H&E-stained colonic pathological sections of mice are shown in Figure 5d, which indicate that the $CCNZ_1$:$Alg_{1.5}$ nanozyme hydrogel group with single dose showed less glandular defects, less inflammatory cell infiltration, and promoted mucosal healing. Collectively, the *in vivo* data showed that the $CCNZ_1$:$Alg_{1.5}$ nanozyme hydrogel exhibited highly therapeutic efficacy even for single dose.

https://doi.org/10.1021/acs.bioconjchem.1c00583
Bioconjugate Chem. 2022, 33, 248−259

CONCLUSIONS

In summary, we developed a nanozyme hydrogel with ROS-scavenging activities and mucosal healing capacity for UC therapy, which exhibits higher therapeutic efficacy than 5-ASA and the state-of-the-art CeO_2 nanozyme. Even though nanozymes have been widely studied,[26] few studies focus on promoting mucosal healing, which plays an important role in UC therapy. By using the dual-cross-linking hydrogel, the CCNZ&Alg nanozyme hydrogel was successfully fabricated. The antibacterial activity and surface charge were rationally regulated by different ratios of CCNZ and Alg. By taking advantage of excellent inflamed site-targeting ability and antibacterial capacity, the nanozyme hydrogel could enhance the residence time and eliminate interference from foreign bacteria in the inflamed sites. With the optimal formulation of the nanozyme hydrogel, the obtained $CCNZ_1$:$Alg_{1.5}$ nanozyme hydrogel was capable to scavenge ROS, exert antibacterial activity, target to the inflamed sites, and support cell growth. For UC therapy, the nanozyme hydrogel not only decreased inflammatory response but also promoted mucosal healing. In addition, the reduction of treatment frequency and dose of the nanozyme hydrogel can also reserve the therapeutic effects and decrease the side effects. Therefore, we propose that the $CCNZ_1$:$Alg_{1.5}$ nanozyme hydrogel could provide an innovative treatment strategy for UC therapy with excellent potential for clinical application. Furthermore, the design-on-demand strategy could be encouraged and achieved with the rational design and synthesis in this work for a broader spectrum of diseases.

METHODS

Materials. Cerium nitrate hexahydrate (99.95%), ethylene glycol (AR, 98%), ammonia solution (AR, 25−28%), 2′,7′-dichlorofluorescein diacetate (DCFH-DA), DSS, and 5-ASA were obtained from Aladdin (Shanghai, China). Chitosan and sodium alginate were obtained from Macklin (Shanghai, China). Deionized (DI) water (18.2 MΩ·cm, Millipore) was used to prepare aqueous solution. Cell Counting Kit (CCK)-8 assay (Dojindo Laboratories, Japan) was utilized to determine cell viability.

Characterization. TEM imaging was carried out using a Tecnai F20 microscope FEI (Field Electron and Iron Company) at an acceleration voltage of 200 kV, and SEM imaging was carried out using a Quanta 200 scanning electron microscope (Quanta 200) at an acceleration voltage of 10 kV. Zeta potential and dynamic light scattering (DLS) were measured on a Nanosizer ZS90 (Malvern). XRD spectra were measured using a Rigaku Ultima diffractometer with 2° min^{-1} using Cu Kα radiation. FTIR spectra were recorded using a Thermo Nicolet Near FTIR NEXUS 870 spectrometer. The dissolved oxygen was monitored using a dissolved oxygen meter (SevenExcellence Multiparameter, METTLER TOLE-DO Co. Ltd.). The amounts of Ce in CCNZ and colon tissues were analyzed by ICP atomic emission spectroscopy (ICP-AES) (Thermo Scientific). Stained cells were analyzed by laser scanning confocal microscopy (OLYMPUS) and flow cytometry (BD Biosciences).

Preparation of CCNZ and CCNZ&Alg Nanozyme Hydrogels. The CCNZ was prepared by the NH_4OH precipitation method. In brief, 10 mL of glycol solution of 12.6 mg/mL $Ce(NO_3)_3{\cdot}6H_2O$ was added into 10 mL of 0.1% acetic acid solution of Cs under vigorous stirring over 5 min at room temperature. Then, 1.6 mL of ammonium hydroxide was quickly injected into the mixture solution under vigorous stirring conditions. After 12 h, the formed CCNZ was collected by centrifugation and washed by DI water, until neutralization of the filtrate solution to physiological pH 7.4. Finally, the products were redispersed in 0.1% acetic acid solution. The nanozyme hydrogels with different compositions ($CCNZ_1$:Alg_1, $CCNZ_1$:$Alg_{1.5}$, $CCNZ_1$:Alg_2, and $CCNZ_1$:Alg_3) were formed with different ratios of CCNZ and alginate (1:1, 1:1.5, 1:2, and 1:3 w/w %), respectively. The mixture was shaken for 10 min.

SOD- and CAT-Mimicking Activity of CCNZ. The SOD-mimicking catalytic activity of CCNZ was investigated with the nitro blue tetrazolium (NBT) probe, and $^{\bullet}O_2^-$ was produced by irradiating riboflavin. Typically, NBT (0.1 mg mL^{-1}), ethylenediaminetetraacetic acid (0.1 M), riboflavin (1.2 mM), and different concentrations of CCNZ or citric acid-coated CeO_2 were mixed in phosphate-buffered saline (PBS) (0.1 M, pH 7.2) at 37 °C for 5 min. Then, the mixtures were irradiated with a light-emitting diode lamp for 2 min. The absorption at the wavelength of 590 nm of the mixed solution was obtained using a microplate reader.

The CAT-mimicking catalytic activity of CCNZ was investigated by monitoring the amount of generated oxygen with a dissolved oxygen meter. Briefly, CCNZ and H_2O_2 were successively added into 6 mL of water. The different concentrations of CCNZ were 5, 10, 20, 40, and 80 μg mL^{-1}, respectively. Also, the final concentration of H_2O_2 was 5 mM. In addition, to investigate the stability of the nanozyme hydrogel in stomach, the nanozyme hydrogel was kept in 0.9% NaCl (pH 1.2 or 6.8) for 4 h, and then, the H_2O_2 elimination efficiency was measured under neutral conditions after 1 or 24 h. Δdissolved oxygen = total dissolved oxygen − dissolved oxygen of H_2O_2 self-decomposition.

Cell Culture. The RAW 264.7 cells were cultured in the high-glucose Dulbecco's modified Eagle medium containing 10% fetal bovine serum and 1% penicillin−streptomycin under a humidified atmosphere of 5% CO_2 at 37 °C.

Cell Viability. After seeding RAW 264.7 cells at a density of 7×10^4 cells in 96-well plates for 24 h, CCNZ with different concentrations (0−100 μg mL^{-1}) was added and incubated for 24 h, followed by washing cells with PBS. The CCK-8 assay was used to evaluate cell viability. For the nanozyme hydrogel, different concentrations of the nanozyme hydrogel were seeded in the transwell cell culture system, the cell viability was evaluated by CCK-8. Besides, after staining with Calcein-AM/PI, the images were obtained with laser scanning confocal microscopy.

ROS-Scavenging Ability of RAW 264.7 Cells. After seeding RAW 264.7 cells at a density of 2×10^5 cells in six-well plates for 24 h, CCNZ was added and further incubated for 2 h. Then, 200 μM H_2O_2 in a fresh medium was added and cultured for 30 min except for the control group. After being incubated with 10 μM DCFH-DA for 20 min and washed with PBS to remove excessive probes, the cells were observed with laser scanning confocal microscopy. Besides, after being stimulated with H_2O_2 and incubated with DCFH-DA, the cells were collected by centrifugation and analyzed by flow cytometry.

Cell Growth on the Nanozyme Hydrogel. In order to investigate the ability of the nanozyme hydrogel to support cell growth, RAW 264.7 cells with a density of 2×10^5 cell mL^{-1} were cultured on the nanozyme hydrogel in 6six-well plates for

https://doi.org/10.1021/acs.bioconjchem.1c00583
Bioconjugate Chem. 2022, 33, 248−259

24 h. Then, after being stained with Calcein-AM/PI, the images were obtained with laser scanning confocal microscopy.

Antibacterial Activity of the Nanozyme Hydrogel. The samples were challenged with *E. coli*/*S. aureus* bacteria at a final concentration of 1×10^5 CFU mL^{-1}. In a 15 mL centrifuge tube, bacteria and the nanozyme hydrogel (100 μL) were cocultured for 4 h at 37 °C. The antibacterial activity was studied using a spread plate, which seeded 50 μL of bacteria and the nanozyme hydrogel stock suspension onto a spread plate. The plate was incubated at 37 °C for 24 h to form viable colony units. Photographs were taken to analyze the antibacterial activity.

Animal Studies. The anesthetic, surgical, and post-operative care protocols were examined and approved by the Animal Ethics Committee of Nanjing Drum Tower Hospital and conducted under the Institutional Committee of Care and Use of Laboratory Animals. Male C57BL/6 mice, with an average bodyweight of 22 g, from the Experimental Animal Center of Nanjing Medical University, were used in this study.

Biocompatibility and Cell Growth *In Vivo*. The *in vivo* host response and cell growth ability were evaluated through subcutaneously embedding the $CCNZ_1$:$Alg_{1.5}$ nanozyme hydrogel or Cs&Alg hydrogel in mice. After 7 days, all mice were sacrificed and the skins where samples were implanted were excised. Then, the inflammatory response and cell growth ability were measured by H&E staining of the skin tissues.

DSS-Induced Model of UC.[24] 22 g male C57BL/6 mice were acclimatized for 1 week before inclusion in this work, and each group had six mice. Mice were fed with sterile water containing 2% (w/v) DSS for consecutive 7 or 8 days. On the 8th day, all groups were replaced with sterile water without DSS, and the mice were orally administered with 5-ASA, CeO_2, Cs&Alg, $CCNZ_1$:$Alg_{1.5}$, and $CCNZ_1$:Alg_2 nanozyme hydrogel, respectively, for treatment. After 3 days' administration or 1 days' administration with 2 days' blank to medicine, all mice were sacrificed. Meanwhile, their colon and internal organs (heart, liver, spleen, lung, and kidney) were collected, sectioned, and stained with H&E, Masson, and AB-PAS. The colon length, *in vivo* anti-inflammation efficiency, fibrosis responses, mucosal healing efficiency, and biocompatibility were recorded.

***Ex Vivo* ROS Evaluation of the Nanozyme Hydrogel.** For *ex vivo* ROS evaluation, the UC model of mice followed the same protocol as mentioned above. After the intraperitoneal injection of DCFH-DA (0.7 mg per mouse) for 0.5 h on day 11, the ROS-scavenging sufficiency of different indicated groups was evaluated by collecting the colons. The fluorescence images of the whole colons were recorded using a PerkinElmer *in vivo* imaging system with an excitation wavelength of 465 nm and an emission wavelength of 520 nm.

Inflammation targeting of the nanozyme hydrogel: first, the CCNZ (20 mg mL^{-1}) was labeled with the FITC fluorescence probe (2 mg mL^{-1}) under magnetic stirring for 12 h at 4 °C in darkness. Then, the CCNZ was dialyzed against DI water for 24 h in a dialysis bag with a molecular weight cutoff of 1000 Da at 4 °C in darkness and collected by centrifugation (12,000 rpm and 10 min) to obtain the FITC-labeled nanozyme hydrogel. Finally, the UC model of mice was established following the same protocol as mentioned above, and the FITC-labeled nanozyme hydrogel was orally administrated. The fluorescence images of the whole colons were recorded using a PerkinElmer *in vivo* imaging system with an excitation wavelength of 465 nm and an emission wavelength of 520 nm.

Besides, the Ce element in the colon tissue was investigated by ICP-AES. First, the parts of colons of all groups were processed by freeze-drying. Then, the products were immersed in concentrated nitric acid for 12 h at 60 °C. The solution was diluted 10 times before being examined by ICP-AES.

■ ASSOCIATED CONTENT

Supporting Information

The Supporting Information is available free of charge at https://pubs.acs.org/doi/10.1021/acs.bioconjchem.1c00583.

DLS profile of CCNZ, elimination efficiency of $^{\bullet}O_2^-$, digital photographs of the remaining bacteria-inoculated agar plates, EDS, H_2O_2 elimination of $CCNZ_1$:$Alg_{1.5}$, nanozyme hydrogel treated in pH 6.8 and 1.2 for 4 h, cytotoxicity of the nanozyme hydrogel evaluated by using a transwell cell culture system, confocal images of RAW 264.7 cells, release of CCNZ from the nanozyme hydrogel, fluorescence images of colon after treatment with the FITC-conjugated $CCNZ_1$:$Alg_{1.5}$ nanozyme hydrogel, images of the colons with indicated treatments and schematic of the method for the measurement of colon length, fluorescence images of colon 0.5 h after injecting 0.7 mg of DCFH-DA per mouse, H&E-stained histology sections, images of the colons with single-dose treatment, and ICP characterization of CCNZ (PDF)

■ AUTHOR INFORMATION

Corresponding Author

Hui Wei − *Department of Biomedical Engineering, College of Engineering and Applied Sciences, Nanjing National Laboratory of Microstructures, Jiangsu Key Laboratory of Artificial Functional Materials, Nanjing University, Nanjing, Jiangsu 210023, China; State Key Laboratory of Analytical Chemistry for Life Science and State Key Laboratory of Coordination Chemistry, School of Chemistry and Chemical Engineering, Chemistry and Biomedicine Innovation Center (ChemBIC), Nanjing University, Nanjing, Jiangsu 210023, China*; orcid.org/0000-0003-0870-7142; Email: weihui@nju.edu.cn

Authors

Chaoqun Cheng − *Department of Biomedical Engineering, College of Engineering and Applied Sciences, Nanjing National Laboratory of Microstructures, Jiangsu Key Laboratory of Artificial Functional Materials, Nanjing University, Nanjing, Jiangsu 210023, China*

Yuan Cheng − *Department of Biomedical Engineering, College of Engineering and Applied Sciences, Nanjing National Laboratory of Microstructures, Jiangsu Key Laboratory of Artificial Functional Materials, Nanjing University, Nanjing, Jiangsu 210023, China*

Sheng Zhao − *Department of Biomedical Engineering, College of Engineering and Applied Sciences, Nanjing National Laboratory of Microstructures, Jiangsu Key Laboratory of Artificial Functional Materials, Nanjing University, Nanjing, Jiangsu 210023, China*

Quan Wang − *Department of Biomedical Engineering, College of Engineering and Applied Sciences, Nanjing National Laboratory of Microstructures, Jiangsu Key Laboratory of Artificial Functional Materials, Nanjing University, Nanjing, Jiangsu 210023, China*

Sirong Li − *Department of Biomedical Engineering, College of Engineering and Applied Sciences, Nanjing National Laboratory of Microstructures, Jiangsu Key Laboratory of Artificial Functional Materials, Nanjing University, Nanjing, Jiangsu 210023, China*

Xiwen Chen − *Department of Biomedical Engineering, College of Engineering and Applied Sciences, Nanjing National Laboratory of Microstructures, Jiangsu Key Laboratory of Artificial Functional Materials, Nanjing University, Nanjing, Jiangsu 210023, China*

Xiaohan Yang − *State Key Laboratory of Pollution Control and Resource Reuse, School of the Environment, Nanjing University, Nanjing, Jiangsu 210023, China*

Complete contact information is available at: https://pubs.acs.org/10.1021/acs.bioconjchem.1c00583

Author Contributions

C.C. and Y.C. contributed equally to this work. C.C. and H.W. designed the experiments. C.C. synthesized the materials, performed the cellular experiment, and performed the *in vitro* and *in vivo* study and analyzed the data. Y.C. designed the *in vivo* animal model and performed the *in vivo* study. S.Z. assisted in synthesizing the materials. Q.W. contributed to SOD-like activity test and analyzed the data. S.Z. and S.L. contributed to the SEM characterization test. X.C. assisted with the animal experiment, and X.Y. assisted with ICP characterization.

Notes

The authors declare no competing financial interest.

■ ACKNOWLEDGMENTS

This work was supported by the National Natural Science Foundation of China (21874067 and 21722503), the Natural Science Foundation of Jiangsu Province (BK20180340), the National Key R&D Program of China (2019YFA0709200), the CAS Interdisciplinary Innovation Team (JCTD-2020-08), the PAPD Program, and the Fundamental Research Funds for the Central Universities (021314380195).

■ REFERENCES

(1) Levesque, B. G.; Sandborn, W. J.; Ruel, J.; Feagan, B. G.; Sands, B. E.; Colombel, J.-F. Converging goals of treatment of inflammatory bowel disease from clinical trials and practice. *Gastroenterology* **2015**, *148*, 37−51.

(2) Mittal, M.; Siddiqui, M. R.; Tran, K.; Reddy, S. P.; Malik, A. B. Reactive oxygen species in inflammation and tissue injury. *Antioxid. Redox Signaling* **2014**, *20*, 1126−1167.

(3) Aviello, G.; Knaus, U. ROS in gastrointestinal inflammation: Rescue Or Sabotage? *Br. J. Pharmacol.* **2017**, *174*, 1704−1718.

(4) Miyachi, Y.; Yoshioka, A.; Imamura, S.; Niwa, Y. Effect of sulphasalazine and its metabolites on the generation of reactive oxygen species. *Gut* **1987**, *28*, 190−195.

(5) Monstad, I. L.; Solberg, I. C.; Cvancarova, M.; Hovde, O.; Henriksen, M.; Huppertz-Hauss, G.; Gunther, E.; Moum, B. A.; Stray, N.; Vatn, M.; et al. Outcome of Ulcerative Colitis 20 Years after Diagnosis in a Prospective Population-based Inception Cohort from South-Eastern Norway, the IBSEN Study. *J. Crohn's Colitis* **2021**, *15*, 969−979.

(6) Marshall, J. K.; Thabane, M.; Steinhart, A. H.; Newman, J. R.; Anand, A.; Irvine, E. J. Rectal 5-aminosalicylic acid for induction of remission in ulcerative colitis. *Cochrane Database Syst. Rev.* **2010**, *1*, Cd004115.

(7) Wei, H.; Wang, E. Nanomaterials with enzyme-like characteristics (nanozymes): next-generation artificial enzymes. *Chem. Soc. Rev.* **2013**, *42*, 6060−6093. Huang, Y.; Ren, J.; Qu, X. Nanozymes: Classification, Catalytic Mechanisms, Activity Regulation, and Applications. *Chem. Rev.* **2019**, *119*, 4357−4412. Wei, H.; Gao, L.; Fan, K.; Liu, J.; He, J.; Qu, X.; Dong, S.; Wang, E.; Yan, X. Nanozymes: A clear definition with fuzzy edges. *Nano Today* **2021**, *40*, 101269. Gao, L.; Zhuang, J.; Nie, L.; Zhang, J.; Zhang, Y.; Gu, N.; Wang, T.; Feng, J.; Yang, D.; Perrett, S.; et al. Intrinsic peroxidase-like activity of ferromagnetic nanoparticles. *Nat. Nanotechnol.* **2007**, *2*, 577−583. Huang, L.; Chen, J.; Gan, L.; Wang, J.; Dong, S. Single-atom nanozymes. *Sci. Adv.* **2019**, *5*, No. eaav5490. Tonga, G. Y.; Jeong, Y.; Duncan, B.; Mizuhara, T.; Mout, R.; Das, R.; Kim, S. T.; Yeh, Y.-C.; Yan, B.; Hou, S.; et al. Supramolecular regulation of bioorthogonal catalysis in cells using nanoparticle-embedded transition metal catalysts. *Nat. Chem.* **2015**, *7*, 597−603. Manea, F.; Houillon, F. B.; Pasquato, L.; Scrimin, P. Nanozymes: gold-nanoparticle-based transphosphorylation catalysts. *Angew. Chem., Int. Ed.* **2004**, *43*, 6165−6169. Zhang, Z.; Zhang, X.; Liu, B.; Liu, J. Molecular Imprinting on Inorganic Nanozymes for Hundred-fold Enzyme Specificity. *J. Am. Chem. Soc.* **2017**, *139*, 5412−5419. Soh, M.; Kang, D.-W.; Jeong, H.-G.; Kim, D.; Kim, D. Y.; Yang, W.; Song, C.; Baik, S.; Choi, I.-Y.; Ki, S.-K.; et al. Ceria-Zirconia Nanoparticles as an Enhanced Multi-Antioxidant for Sepsis Treatment. *Angew. Chem., Int. Ed.* **2017**, *56*, 11399−11403. Loynachan, C. N.; Soleimany, A. P.; Dudani, J. S.; Lin, Y.; Najer, A.; Bekdemir, A.; Chen, Q.; Bhatia, S. N.; Stevens, M. M. Renal clearable catalytic gold nanoclusters for in vivo disease monitoring. *Nat. Nanotechnol.* **2019**, *14*, 883−890. Zhang, W.; Hu, S.; Yin, J.-J.; He, W.; Lu, W.; Ma, M.; Gu, N.; Zhang, Y. Prussian Blue Nanoparticles as Multienzyme Mimetics and Reactive Oxygen Species Scavengers. *J. Am. Chem. Soc.* **2016**, *138*, 5860−5865. Komkova, M. A.; Karyakina, E. E.; Karyakin, A. A. Catalytically Synthesized Prussian Blue Nanoparticles Defeating Natural Enzyme Peroxidase. *J. Am. Chem. Soc.* **2018**, *140*, 11302−11307. Xi, Z.; Cheng, X.; Gao, Z.; Wang, M.; Cai, T.; Muzzio, M.; Davidson, E.; Chen, O.; Jung, Y.; Sun, S.; et al. Strain Effect in Palladium Nanostructures as Nanozymes. *Nano Lett.* **2020**, *20*, 272−277.

(8) Zhao, J.; Cai, X.; Gao, W.; Zhang, L.; Zou, D.; Zheng, Y.; Li, Z.; Chen, H. Prussian Blue Nanozyme with Multienzyme Activity Reduces Colitis in Mice. *ACS Appl. Mater. Interfaces* **2018**, *10*, 26108−26117. Cheng, Y.; Cheng, C.; Yao, J.; Yu, Y.; Liu, Y.; Zhang, H.; Miao, L.; Wei, H. Mn_3O_4 Nanozyme for Inflammatory Bowel Disease Therapy. *Adv. Ther.* **2021**, *4*, 2100081.

(9) Liu, Y.; Cheng, Y.; Zhang, H.; Zhou, M.; Yu, Y.; Lin, S.; Jiang, B.; Zhao, X.; Miao, L.; Wei, C. W.; et al. Integrated cascade nanozyme catalyzes in vivo ROS scavenging for anti-inflammatory therapy. *Sci. Adv.* **2020**, *6*, No. eabb2695.

(10) Tirosh, B.; Khatib, N.; Barenholz, Y.; Nissan, A.; Rubinstein, A. Transferrin as a luminal target for negatively charged liposomes in the inflamed colonic mucosa. *Mol. Pharm.* **2009**, *6*, 1083−1091.

(11) Zhao, J.; Gao, W.; Cai, X.; Xu, J.; Zou, D.; Li, Z.; Hu, B.; Zheng, Y. Nanozyme-mediated catalytic nanotherapy for inflammatory bowel disease. *Theranostics* **2019**, *9*, 2843−2855.

(12) Zhao, S.; Li, Y.; Liu, Q.; Li, S.; Cheng, Y.; Cheng, C.; Sun, Z.; Du, Y.; Butch, C. J.; Wei, H. An Orally Administered CeO_2@ Montmorillonite Nanozyme Targets Inflammation for Inflammatory Bowel Disease Therapy. *Adv. Funct. Mater.* **2020**, *30*, 2004692.

(13) Boal Carvalho, P.; Cotter, J. Mucosal Healing in Ulcerative Colitis: A Comprehensive Review. *Drugs* **2017**, *77*, 159−173.

(14) Rosenberg, L.; Lawlor, G. O.; Zenlea, T.; Goldsmith, J. D.; Gifford, A.; Falchuk, K. R.; Wolf, J. L.; Cheifetz, A. S.; Robson, S. C.; Moss, A. C. Predictors of endoscopic inflammation in patients with ulcerative colitis in clinical remission. *Inflamm. Bowel Dis.* **2013**, *19*, 779−784.

(15) Antoni, L.; Nuding, S.; Weller, D.; Gersemann, M.; Ott, G.; Wehkamp, J.; Stange, E. F. Human colonic mucus is a reservoir for antimicrobial peptides. *J. Crohn's Colitis* **2013**, *7*, e652−e664. Nuding, S.; Fellermann, K.; Wehkamp, J.; Stange, E. F. Reduced mucosal antimicrobial activity in Crohn's disease of the colon. *Gut* **2007**, *56*, 1240−1247.

(16) Frøslie, K. F.; Jahnsen, J.; Moum, B. A.; Vatn, M. H. Mucosal healing in inflammatory bowel disease: results from a Norwegian population-based cohort. *Gastroenterology* **2007**, *133*, 412−422. Neurath, M. F.; Leppkes, M. Resolution of ulcerative colitis. *Semin. Immunopathol.* **2019**, *41*, 747−756.
(17) Baldim, V.; Yadav, N.; Bia, N.; Graillot, A.; Loubat, C.; Singh, S.; Karakoti, A. S.; Berret, J.-F. Polymer-Coated Cerium Oxide Nanoparticles as Oxidoreductase-like Catalysts. *ACS Appl. Mater. Interfaces* **2020**, *12*, 42056−42066. Mitra, R. N.; Gao, R.; Zheng, M.; Wu, M.-J.; Voinov, M. A.; Smirnov, A. I.; Smirnova, T. I.; Wang, K.; Chavala, S.; Han, Z. Glycol Chitosan Engineered Autoregenerative Antioxidant Significantly Attenuates Pathological Damages in Models of Age-Related Macular Degeneration. *ACS Nano* **2017**, *11*, 4669−4685.
(18) Zeng, F.; Wu, Y.; Li, X.; Ge, X.; Guo, Q.; Lou, X.; Cao, Z.; Hu, B.; Long, N. J.; Mao, Y.; et al. Custom-Made Ceria Nanoparticles Show a Neuroprotective Effect by Modulating Phenotypic Polarization of the Microglia. *Angew. Chem., Int. Ed.* **2018**, *57*, 5808−5812.
(19) Baldim, V.; Yadav, N.; Bia, N.; Graillot, A.; Loubat, C.; Singh, S.; Karakoti, A. S.; Berret, J.-F. Polymer-Coated Cerium Oxide Nanoparticles as Oxidoreductase-like Catalysts. *ACS Appl. Mater. Interfaces* **2020**, *12*, 42056−42066.
(20) Trujillo-Reyes, J.; Vilchis-Nestor, A. R.; Majumdar, S.; Peralta-Videa, J. R.; Gardea-Torresdey, J. L. Citric acid modifies surface properties of commercial CeO_2 nanoparticles reducing their toxicity and cerium uptake in radish (Raphanus sativus) seedlings. *J. Hazard. Mater.* **2013**, *263*, 677−684. Barrios, A. C.; Rico, C. M.; Trujillo-Reyes, J.; Medina-Velo, I. A.; Peralta-Videa, J. R.; Gardea-Torresdey, J. L. Effects of uncoated and citric acid coated cerium oxide nanoparticles, bulk cerium oxide, cerium acetate, and citric acid on tomato plants. *Sci. Total Environ.* **2016**, *563*−*564*, 956−964.
(21) Irving, P. M.; Gibson, P. R. Infections and IBD. *Nat. Clin. Pract. Gastroenterol. Hepatol.* **2008**, *5*, 18−27.
(22) Zhao, X.; Xia, Y.; Li, Q.; Ma, X.; Quan, F.; Geng, C.; Han, Z. Microwave-assisted synthesis of silver nanoparticles using sodium alginate and their antibacterial activity. *Colloids Surf., A* **2014**, *444*, 180−188.
(23) Rota, C.; Chignell, C. F.; Mason, R. P. Evidence for free radical formation during the oxidation of 2'-7'-dichlorofluorescin to the fluorescent dye 2'-7'-dichlorofluorescein by horseradish peroxidase: possible implications for oxidative stress measurements. *Free Radic. Biol. Med.* **1999**, *27*, 873−881.
(24) Wirtz, S.; Neufert, C.; Weigmann, B.; Neurath, M. F. Chemically induced mouse models of intestinal inflammation. *Nat. Protoc.* **2007**, *2*, 541−546.
(25) Azuma, K.; Osaki, T.; Ifuku, S.; Saimoto, H.; Tsuka, T.; Imagawa, T.; Okamoto, Y.; Minami, S. alpha-Chitin nanofibrils improve inflammatory and fibrosis responses in inflammatory bowel disease mice model. *Carbohydr. Polym.* **2012**, *90*, 197−200.
(26) Cheng, C.; Zhao, S.; Cheng, Y.; Liu, Y.; Wei, H. Design of nanozymes for inflammatory bowel disease therapy. *Sci. China Life Sci.* **2021**, *64*, 1368−1371.

https://doi.org/10.1021/acs.bioconjchem.1c00583
Bioconjugate Chem. 2022, 33, 248−259